

Article

Methods for the Construction and Editing of an Efficient Control Network for the Photogrammetric Processing of Massive Planetary Remote Sensing Images

Xin Ma ^{1,2,3}, Chun Liu ^{1,3}, Xun Geng ^{2,3,*}, Sifen Wang ^{4,5}, Tao Li ⁵, Jin Wang ^{2,3}, Pengying Liu ^{2,3}, Jiujiang Zhang ^{2,3}, Qiudong Wang ^{1,2,3}, Yuying Wang ^{2,3}, Yinhui Wang ^{2,3} and Zhen Peng ^{2,3}

¹ School of Computer and Information Engineering, Henan University, Kaifeng 475004, China; maxin@henu.edu.cn (X.M.); liuchun@henu.edu.cn (C.L.); wangqiudong@henu.edu.cn (Q.W.)

² College of Geography and Environmental Science, Henan University, Kaifeng 475004, China; wangjin@henu.edu.cn (J.W.); liupy@henu.edu.cn (P.L.); zhangjiujiang@henu.edu.cn (J.Z.); wyyw@henu.edu.cn (Y.W.); wangyinhui@henu.edu.cn (Y.W.); pengzhen0617@henu.edu.cn (Z.P.)

³ State Key Laboratory of Geo-Information Engineering, Xi'an 710054, China

⁴ School of Transportation Science and Engineering, Beihang University, Beijing 100191, China; sfwang@buaa.edu.cn

⁵ Beijing Institute of Control Engineering, Beijing 100090, China; litao11@henu.edu.cn

* Correspondence: gengxun@henu.edu.cn

Abstract: Planetary photogrammetry remains an important technical means of producing high-precision planetary maps. High-quality control networks are fundamental to successful bundle adjustment. However, current software tools used by the planetary mapping community to construct and edit control networks exhibit very low efficiency. Moreover, redundant and invalid control points in the control network can further increase the time required for the bundle adjustment process. Due to a lack of targeted algorithm optimization, existing software tools and methods are unable to meet the photogrammetric processing requirements of massive planetary remote sensing images. To address these issues, we first proposed an efficient control network construction framework based on approximate orthoimage matching and hash quick search. Next, to effectively reduce the redundant control points in the control network and decrease the computation time required for bundle adjustment, we then proposed a control network-thinning algorithm based on a K-D tree fast search. Finally, we developed an automatic detection method based on ray tracing for identifying invalid control points in the control network. To validate the proposed methods, we conducted photogrammetric processing experiments using both the Lunar Reconnaissance Orbiter (LRO) narrow-angle camera (NAC) images and the Origins Spectral Interpretation Resource Identification Security Regolith Explorer (OSIRIS-REx) PolyCam images; we then compared the results with those derived from the famous open-source planetary photogrammetric software, the United States Geological Survey (USGS) Integrated Software for Imagers and Spectrometers (ISIS) version 8.0.0. The experimental results demonstrate that the proposed methods significantly improve the efficiency and quality of constructing control networks for large-scale planetary images. For thousands of planetary images, we were able to speed up the generation and editing of the control network by more than two orders of magnitude.



Citation: Ma, X.; Liu, C.; Geng, X.; Wang, S.; Li, T.; Wang, J.; Liu, P.; Zhang, J.; Wang, Q.; Wang, Y.; et al. Methods for the Construction and Editing of an Efficient Control Network for the Photogrammetric Processing of Massive Planetary Remote Sensing Images. *Remote Sens.* **2024**, *16*, 4600. <https://doi.org/10.3390/rs16234600>

Academic Editor: Giancarlo Bellucci

Received: 9 October 2024

Revised: 2 December 2024

Accepted: 5 December 2024

Published: 7 December 2024



Copyright: © 2024 by the authors. Licensee MDPI, Basel, Switzerland. This article is an open access article distributed under the terms and conditions of the Creative Commons Attribution (CC BY) license (<https://creativecommons.org/licenses/by/4.0/>).

Keywords: planetary photogrammetry; bundle adjustment; control network; hash table; K-D tree

1. Introduction

In the field of deep space exploration, planetary photogrammetry plays a crucial role in obtaining accurate topographic information regarding extraterrestrial bodies [1]. Planetary maps such as digital orthophoto maps (DOMs) and digital elevation models (DEMs) are essential for analyzing the topography and geomorphology of extraterrestrial

bodies, identifying potential landing sites, and conducting scientific investigations [2]. Currently, artificial intelligence (AI)-based 3D reconstruction technologies such as convolutional neural networks (CNNs), neural radiance fields (NeRFs), and 3D Gauss splitting have demonstrated powerful abilities in the field of computer vision [3–7]. However, in the field of planetary mapping, the photogrammetry technique is still the most reliable method within engineering for generating high-precision mapping products for extraterrestrial bodies. Spacecrafts rely on their navigation systems and attitude sensors to obtain initial exterior orientation (EO) information for planetary remote sensing images [8,9]. Due to errors in the measurement of the spacecraft's orbit and attitude and various differences in imaging conditions, the accuracy of the initial EO information often fails to meet the requirements of high-precision mapping [10,11]. Thus, it is usually necessary to perform bundle adjustments to further refine the initial EO information of planetary images. The key to a successful bundle adjustment lies in constructing a precise and evenly distributed control network [12]. A control network is composed of multiple control points that correspond to specific physical locations on the ground surface. A control measure is a feature point on an image. Each control point can be measured in multiple overlapping images. In other words, one control point contains multiple control measures. The control points in planetary photogrammetry are similar to the tie points in traditional photogrammetry. The control network is usually obtained by means of automatic image matching. However, large-scale photogrammetric projects often require some manual editing to improve the quality of their control network. In the USGS ISIS system, a control network initially comprises 2D-pixel coordinates of control measures but can later be processed to generate 3D ground coordinates for each control point through triangulation and bundle adjustment. Our method follows this convention used in USGS ISIS, and the constructed control network can be seamlessly integrated with USGS ISIS modules.

Recently, vast raw planetary image data have been acquired by mapping cameras onboard the spacecraft of various deep space exploration missions. Due to the limited processing capabilities of existing planetary photogrammetric software, these valuable planetary remote sensing images cannot be processed in a timely manner [13]. For example, approximately 90,000 images returned by the Mars Reconnaissance Orbiter (MRO) Context Camera (CTX) have almost covered the whole surface of Mars. However, the photogrammetric processing of MRO CTX images on a global scale has not yet been achieved, primarily because existing software tools and methods are unable to handle such a large-scale planetary photogrammetric project [14,15]. Additionally, the Lunar Reconnaissance Orbiter (LRO) has acquired more than two million narrow-angle camera (NAC) images with a spatial resolution of 0.8~1.5 m per pixel, and among them, hundreds of thousands of images covered the lunar South Pole (LSP). The LSP has become a key focus of deep space exploration missions for many space agencies, and they are in urgent need of higher-resolution mapping products. Unfortunately, researchers still encounter great challenges in generating large-scale sub-meter-resolution mapping products for the LSP [16–19]. The National Aeronautics and Space Administration (NASA)'s first asteroid exploration mission, the Near-Earth Asteroid Rendezvous (NEAR), acquired over 160,000 images of the near-earth asteroid Eros. The first asteroid sampling and return mission of NASA, Origins Spectral Interpretation Resource Identification Security Regolith Explorer (OSIRIS-REx), spent more than one year on remote sensing observation and collected a large number of images for asteroid Bennu [20–22]. The photogrammetric processing of these massive images of small bodies involves several challenges, such as the effective projection of maps and the efficient construction of control networks for irregularly shaped celestial bodies, which are unique to asteroid mapping [23].

In practical planetary photogrammetric projects, the construction of a control network requires image matching of a large number of stereopairs [24]. Due to the changes in both photographing time and the illumination conditions, there are great differences in the appearance between stereo images. This leads to difficulty in image matching and in automatically generating the control network. Indeed, the most time-consuming tasks

in planetary photogrammetric projects are the generation and editing of their control networks. Moreover, the initial control network derived from image matching often contains redundant and invalid control points, and thinning or manual editing is required to improve the quality. In fact, it always takes several months or even years to complete large-scale planetary photogrammetric projects (e.g., global mapping for the Moon and Mars) [25,26].

In the field of Earth observation, pieces of commercial photogrammetric software such as Trimble Inpho 12.1.1, Bentley Context Capture 10.20, and Agisoft Metashape (formerly known as Photoscan) 2.1.3, as well as free or open-source solutions, including COLMAP 3.8 and OpenMVS 2.3.1, demonstrate a high degree of automation in constructing control networks for drone and satellite images [27–31]. However, these software tools cannot be directly used to process planetary images mainly due to the unsupported format of planetary image data and planetary coordinate systems. Moreover, photogrammetric software in the field of Earth observation always adopts rational polynomial coefficients (RPCs) to process satellite images [32,33]. However, rigorous sensor models are preferred in planetary photogrammetry. Their main advantage is that they have a physical form and can produce mapping products with higher geometric accuracy [34,35]. In the planetary mapping community, there is still a lack of software tools that are able to support the efficient construction and editing of control networks for massive planetary remote sensing images. The Integrated System for Imagers and Spectrometers (ISIS), developed by the United States Geological Survey (USGS), is a well-known form of planetary photogrammetry software [36,37]. It provides a number of tools for the construction of control networks, such as autoseed, cnetref, and pointreg. However, these tools within the software in USGS ISIS always show relatively low efficiency and require some manual intervention [38]. In addition, USGS ISIS also provides several software tools (e.g., qnet and cneteditor) for the editing of the control network. Such editing tools suffer from the same inefficiency as tools for the control network's construction. Indeed, the existing process of constructing and editing the control network based on tools provided by USGS ISIS always involves a large number of manual operations, and it greatly relies on the experiences of the photogrammetric engineers. Another piece of planetary photogrammetric software developed by NASA, namely the Ames Stereo Pipeline (ASP), has optimized the construction of the control network based on parallel computing of multi-threading or multiple machines [39]. However, it has not yet been optimized at the core algorithmic level, so it still cannot function optimally in the photogrammetric processing of massive planetary images. In a word, existing planetary photogrammetry software tools and methods often suffer from low efficiency, excessive manual editing, and limited processing capability. To effectively utilize planetary image data to generate high-precision mapping products, it is necessary to further develop algorithms for the automatic construction of control networks [40].

The generation of a control network usually requires two steps: one is to obtain the corresponding feature point matching files of all image pairs through image matching; the other is to build a control network file that can be directly used in the following bundle adjustment process, based on the previously matched files. Thus far, most researchers have focused on the first step, and the efficiency of image matching, especially for large image sets, might be improved. Existing efficient matching solutions include reducing the number of image pairs and feature points per image and matching multiple images simultaneously [24]. However, there are few studies involving the second step. In this paper, we aim to improve the efficiency of the construction of control networks for massive planetary images, provided that the requisite feature point matching files have been obtained. In this study, we propose efficient methods for the construction and editing of control networks for massive planetary remote sensing images, aiming to enhance their geometric processing ability and degree of automation for large-scale planetary photogrammetric projects. The main contributions of this paper are as follows:

- (1) Firstly, we propose a framework for control network construction based on image matching on approximate orthoimages and hash fast search. Specifically, a unique

hash key is generated for each control measure using a hashing process, and a hash lookup is conducted to quickly identify and eliminate duplicate control points. This allows for the efficient integration of control points into the control network, which can also serve as a solution through which to achieve interoperability in the planetary photogrammetry software.

- (2) Secondly, we introduce a control network-thinning algorithm based on K-D tree spatial indexing, which effectively reduces redundant control points in the control network. It can significantly decrease the computational load involved in subsequent bundle adjustments.
- (3) Finally, we introduce an automated detection method for identifying invalid control points that cannot be calculated with initial three-dimensional ground coordinates, thereby reducing manual editing during the bundle adjustment process.

The structure of this paper is arranged as follows: Section 2.1 introduces the common methods for constructing a control network from massive planetary remote sensing images, including the USGS ISIS method. Section 2.2 presents our proposed hash-based rapid construction method, while Sections 2.3 and 2.4 propose algorithms for handling redundant points and invalid control points within the control network. Section 3 demonstrates the experimental results, including the algorithm's efficiency and the final geometric accuracy. Finally, Section 4 summarizes the conclusions of this work.

2. Control Network Construction and Editing for Massive Planetary Remote Sensing Images

2.1. Conventional Methods of Constructing the Control Network

Figure 1 shows the overall process of constructing the control network. First, the overlapping relationships among all images are calculated. Next, all image pairs (i.e., stereopairs) are matched using feature matching algorithms such as scale-invariant feature transform (SIFT) [41], and the matched feature point (i.e., control point) files are generated for each stereopair. Then, all control points from the generated matched files are merged, and duplicate control measures and control points are removed using an exhaustive search method or the optimized method proposed in this paper. Finally, a control network file, such as a Parameter Value Language (PVL) file supported in USGS ISIS, is generated. This control network file is then used as input in the subsequent bundle adjustment process.

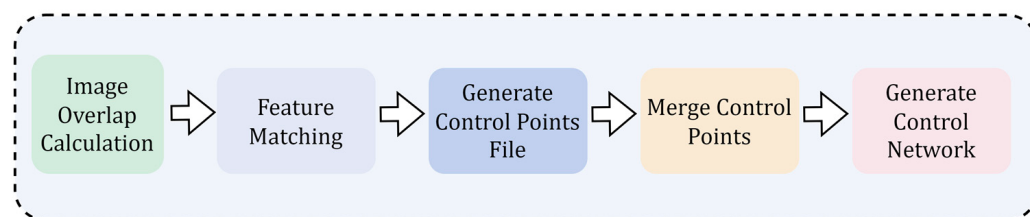


Figure 1. The overall process of constructing the control network.

Figure 2 further illustrates the process of control network construction through merging duplicate control points, provided that the feature point pairs have been obtained by image matching. It should be noted that during image matching, a feature point on one image (i.e., a control measure) may match with multiple feature points on other overlapping images. Currently, most image-matching software modules will generate a matching file for each image pair. Thus, the same feature point on the multi-view overlapping images will be recorded in multiple matching files. Then, the same feature point in an image becomes a control measure of different control points in the following stage of the control network's construction. Therefore, when constructing the control network, these duplicate control points must be merged to ensure the uniqueness of a control measure. More specifically, a control measure on an image should only correspond to one control point in the control network, as demonstrated in Figure 2. Typically, an exhaustive search method is used to merge duplicate control points.

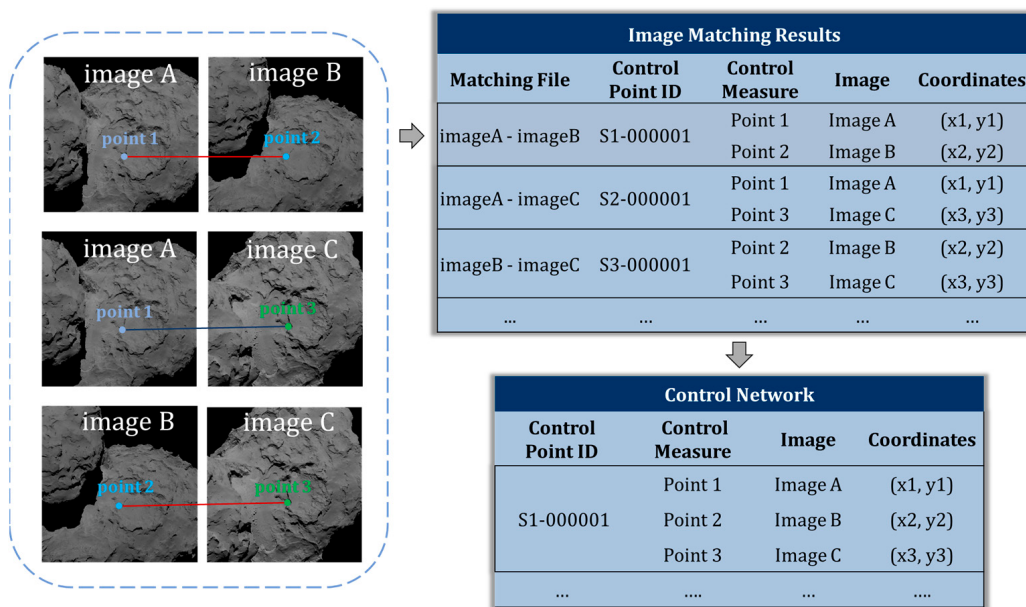


Figure 2. Schematic diagram of the control network construction process after image matching to obtain control points. Since the three control points shown in the left part of the figure are corresponding points, they need to be merged into a single control point.

The workflow of merging control points based on an exhaustive search method is shown in Figure 3. During the process of constructing a control network, we first match each stereopair and yield multiple matching files that record the pixel coordinates of corresponding feature points for each stereopair. During the initialization stage of the control network's construction, the threshold of tolerance for differences in pixel coordinates, σ , can be customized (e.g., 0.1 pixels), and the matching files are used as inputs. Then, all control points in the matching files are processed sequentially to generate a final control network file. For the current control point, we can obtain the pixel coordinates of two control measures on the reference and target images (i.e., a stereopair). Subsequently, the pixel coordinates of control measures on current control points are compared with the pixel coordinates of control measures on other merged control points in the control network. If the differences in pixel coordinates are below the threshold of tolerance σ , the current control point is considered a duplicate control point and needs to be merged with existing control points in the control network. Otherwise, the current control point is directly incorporated into the control network as a new control point. More specifically, if the current control point is a duplicate, the duplicate control measures on the current control point will be discarded, and the non-duplicate control measure will be added to the corresponding existing control point in the control network. Finally, when all control points in the matching files have been processed, the final control network file with no duplicate control points is generated. Obviously, when there are a large number of control points involved in a control network, the process of constructing the control network based on such an exhaustive search will be very time-consuming. This is because the exhaustive search method needs to compare the pixel coordinates of the current control points with the pixel coordinates of all control points in the control network being generated. Thus, this method has very low computational efficiency, making it unsuitable for handling large-scale planetary remote sensing images.

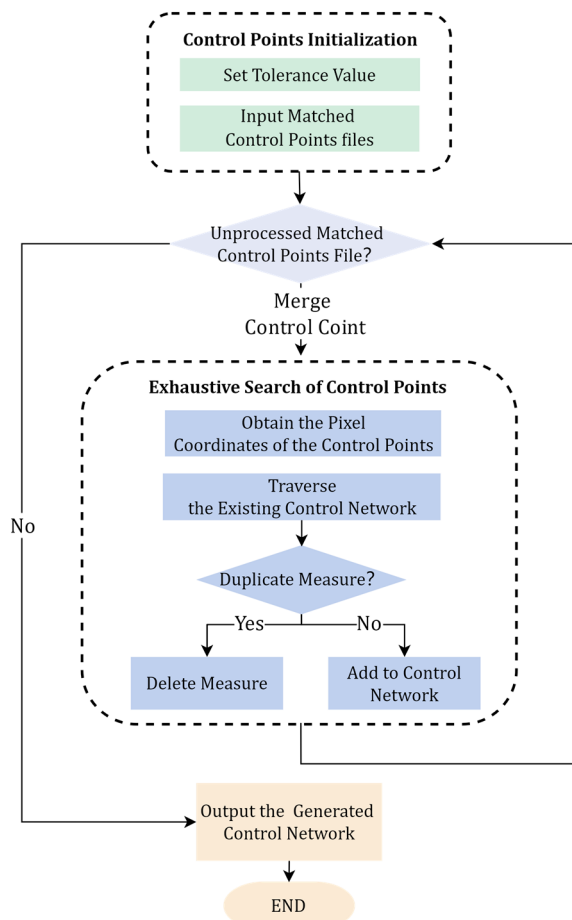


Figure 3. Flowchart of control network construction using the exhaustive search method.

In traditional approaches, apart from the commonly used methods mentioned earlier, the ISIS method is also widely applied in the construction of control networks. USGS ISIS provides several tools for control network construction. The ‘autoseed’ tool automatically generates an initial control network by dividing a grid based on the initial exterior orientation (EO) parameters of the images. Then, ‘pointreg’ uses the normalized cross-correlation (NCC) method to match the corresponding feature points in each grid. However, the NCC matching operation relies heavily on the accuracy of the initial EO parameters to provide a start position from which to search for corresponding feature points. If the EO parameters are inaccurate, a large search window (e.g., 100×100) is required, and the matching process will be time-consuming and can sometimes lead to mismatches. The ‘findfeatures’ software tool uses a feature-matching method to obtain feature point pairs. It iteratively adds control points into a control network by traversing all stereopairs. However, the process of traversing a large number of stereopairs is inefficient. Consequently, these software tools in USGS ISIS face issues with low computational efficiency and mismatches when handling large-scale planetary images.

2.2. A Framework for the Efficient Construction of a Control Network Based on Approximate Orthoimage Matching and Hash Table Quick Search

In this paper, we propose an efficient control network construction framework based on image matching on approximate orthoimages and hash quick search, which significantly enhances the quality and efficiency of control networks constructed from massive planetary remote sensing images. Orthoimages have undergone geometric correction, which is beneficial for consistent image resolution of stereopairs and for removing various distortions. In addition, based on the geometric coordinates of orthophotos, a more reasonable initial

search location can be given for the reference control measure, which can significantly decrease the search range of the matching process. These factors make the image matching on orthophotos exhibit obvious advantages for planetary images. To improve the efficiency with which duplicate control points are queried in the construction of the control network, we designed a standardized naming method to generate a unique hash key for each control measure. The process of generating hash keys is illustrated in Figure 4a. A control point contains multiple control measures, and a control measure is associated with an image. Existing control network construction methods (e.g., USGS ISIS) typically store the original image file name with a control measure. For large photogrammetric projects with millions of control points, the lengthy file names of images will occupy too much storage space. We first used a hashing process to map the lengthy image file name to an eight-digit image sequence number to optimize storage space and computational efficiency. To facilitate the hashing processing and ensure sub-pixel accuracy, we first magnified the floating-point pixel coordinates of control measures by 100 times and then rounded them to the nearest integral number. We then combined the previously generated image sequence number and the rounded pixel coordinates into a single string to serve as the hash key for the control measure. Next, we generated a unique hash value corresponding to the hash key of the control measure using a hash function. As shown in Figure 4b, when a control point is merged into the control network, the control measures' hash keys and the corresponding hash values are imported into the hash table. Note that the same hash key can be generated for the same control measure. Thus, when merging a control point into the control network, we can use the efficient hash search algorithm to identify duplicate control measures and control points.

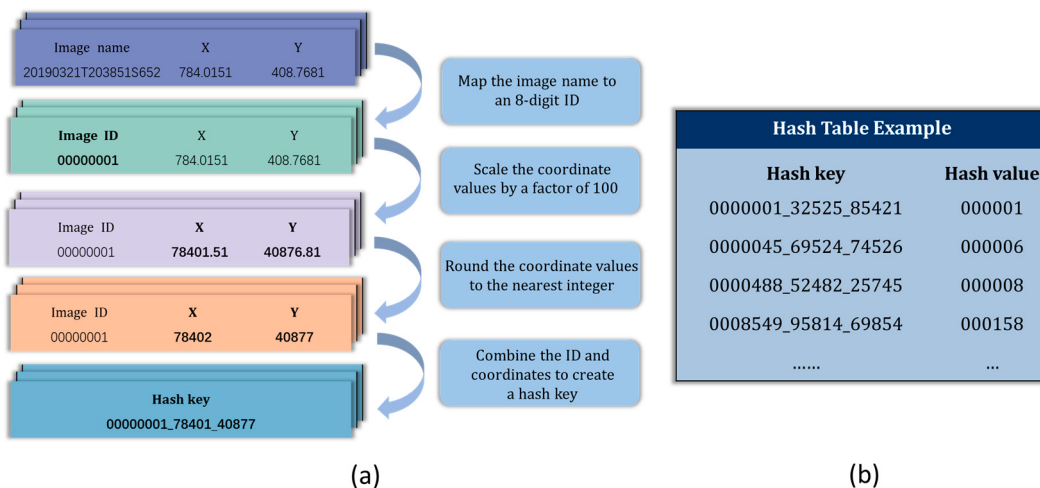


Figure 4. Hash key generation process (a) and example of a hash table (b). The hash key represents the ID of the control measure. If the hash values of two control measures are the same, they belong to the same control point.

The overall processing flow of the proposed control network construction framework is shown in Figure 5.

- (1) Initially, approximate orthoimages were generated using initial EO parameters and existing low-resolution DEM.
- (2) Then, based on these approximate orthoimages, we performed image matching to acquire corresponding feature point pairs, and the pixel coordinates of the matched feature points were then backprojected from the orthophoto space to the original image space [10]. For each stereopair, a matching file was generated. Usually, each line in the matching file stores the pixel coordinates of two control measures corresponding to the same feature point on the reference and target images of the stereopair.

- (3) Then, we initiated the construction of a control network through merging control points. The hash key for each control measure of the control points was generated using the methods mentioned above.
- (4) For a control point currently being merged, we conducted a quick query in the hash table constructed from the previously merged control points; we conducted it using the control measure's hash key. If the hash keys of both control measures in a control point are not found in the hash table, neither control measures have been merged into the control network during previous merging operations. Thus, this control point can be considered a new control point and directly merged into the control network. If the hash key of one control measure is found in the hash table, this control measure has been integrated into the control network during previous rounds of processing. Thus, we used the corresponding hash value in the hash table to add another control measure (the non-duplicate one) into the corresponding control point in the control network. If the hash keys of both control measures are found in the hash table, both control measures have been merged into the control network during previous rounds of processing. As a consequence, these two control measures do not need to be merged into the control network, and the currently merging control point can be directly discarded.
- (5) In the process of merging control points, if there were new control measures or control points merged into the control network, the hash table must be updated.
- (6) Once all control points are processed, they result in a final control network file in PVL file format that can be supported in USGS ISIS.

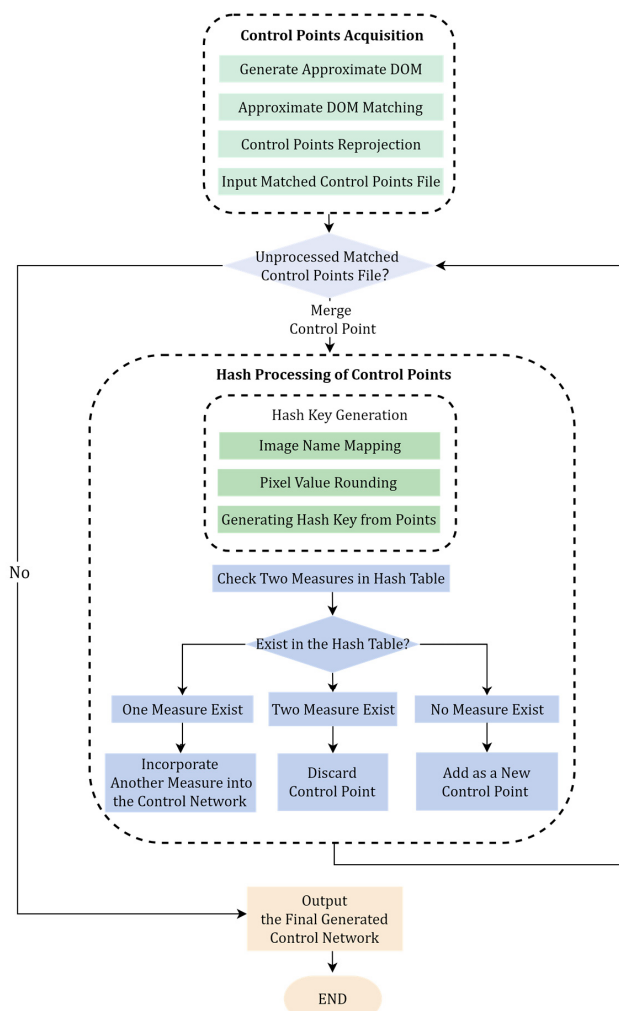


Figure 5. Flowchart of control network construction based on hash processing.

As explained in the previous sections, the computational efficiency of the control network's construction based on an exhaustive search algorithm decreases greatly with an increase in the number of control points, N. Indeed, the algorithmic complexity of the exhaustive search method approaches $O(N^2)$. In contrast, the algorithmic complexity of the hash search method is typically a constant time, $O(1)$. Thus, the proposed control network construction method is very efficient. Previous studies have shown that image matching on approximate images facilitates the acquisition of high-quality control points. This is because this image-matching strategy can eliminate image distortions and make the resolution of the matching images consistent. It is particularly well suited to planetary remote sensing images featuring no moving objects [42]. In fact, software interoperability is inevitable in large-scale photogrammetric projects. Thus, the method of control network construction proposed herein may be considered a framework that can easily parse matching files derived from other forms of image-matching software. It also serves as a basis for more commercial and open-source photogrammetry software to be developed for the fusion processing of massive planetary remote sensing images.

2.3. Control Network Thinning Based on K-D Tree

Redundant control points not only fail to enhance the accuracy of bundle adjustment but also significantly decrease its computational efficiency, particularly during iterative bundle adjustment within large-scale planetary images. Therefore, it is necessary to eliminate excessively redundant control points to improve overall processing efficiency. USGS ISIS features tools that are capable of removing redundant control points. For example, 'qnet' allows for the elimination of control points based on the control point's ID number. However, without prior information, it is difficult to determine which points are redundant, making this function impractical for use. Another function provided by 'qnet' is the removal of control points based on reprojection errors derived from bundle adjustment results. On one hand, this requires bundle adjustment to be carried out in advance with a large number of redundant control points. On the other hand, in some cases, control points with large reprojection errors may be correct image matches and therefore cannot be removed. The main reason for this situation is that the large reprojection errors of control points may be caused by an incorrect mathematical model (including both a functional model and a stochastic model) being used in the bundle adjustment process. Thus, the control network thinning method based on reprojection errors has its limitations. Additionally, 'qnet' also provides a control network thinning function based on spatial distance. It first calculates the spatial distance among control points in the control network and then uses a distance threshold to determine if a control point needs to be kept. Analysis of the USGS ISIS source code reveals that the algorithmic complexity of this method is $O(N^2)$, where N is the number of control points. Indeed, it uses an exhaustive search method to thin the control network, and clearly, its computational efficiency is extremely low when the number of control points is very large. Typically, this method makes it very difficult to conduct thinning operations on control networks with more than ten thousand control points using a regular computer (with an Intel Core i7 CPU and 16GB RAM).

In this study, we present a control network thinning algorithm based on the K-D tree fast search, aiming to efficiently remove redundant control points within the control network. The algorithm workflow is illustrated in Figure 6.

- (1) First, the three-dimensional ground coordinates of the control points are computed based on the initial EO parameters and low-resolution DEM of the celestial body. Specifically, each control measure can intersect with the low-resolution DEM and produce a three-dimensional ground coordinate for the control measure. Then, the final three-dimensional ground coordinates of a control point are obtained by averaging all three-dimensional ground coordinates of the control measures.
- (2) Next, a K-D tree-based data structure is constructed using the three-dimensional ground coordinates of the control points in the control network. Afterward, the processing status of each control point is initialized and marked as unprocessed.

- (3) Subsequently, a neighborhood range R is defined. During the thinning process, the processing status of each control point is first checked. If its status is unprocessed, the process continues to the next step; otherwise, the control point is skipped.
- (4) For an unprocessed control point, the K-D tree search algorithm is used to determine whether any other control points exist within the neighborhood range of this control point. If other control points are found within the search range, they are considered redundant control points. These redundant control points will then be removed, and their status marked as processed. Meanwhile, the current control point is retained in the control network, and its status is marked as processed. If no redundant control points are found within the search radius, the current control point is retained and marked as processed.
- (5) When all control points have been processed, the thinned control network is generated for subsequent use in the bundle adjustment process.

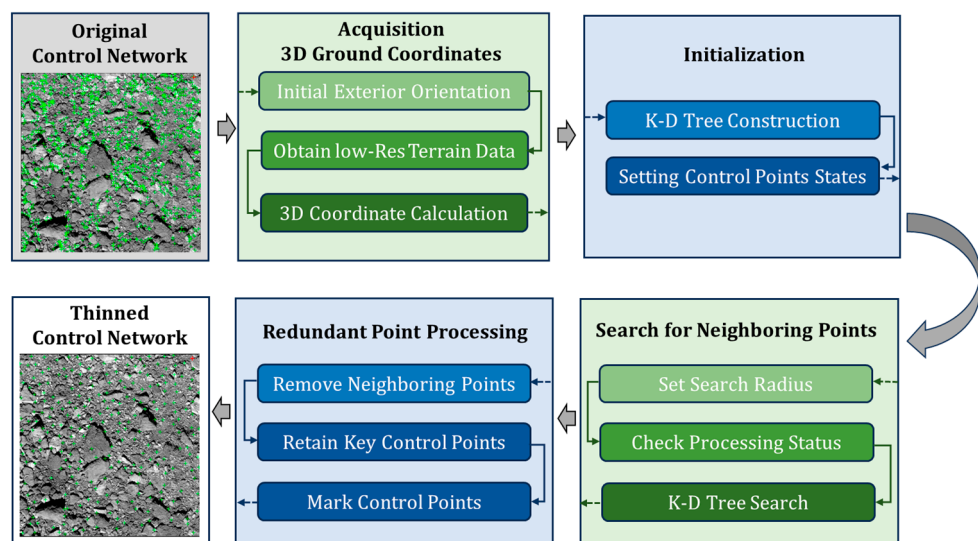


Figure 6. Workflow of the K-D tree thinning algorithm (having acquired 3D ground coordinates).

The proposed control network thinning algorithm creates an efficient K-D tree data structure using the three-dimensional ground coordinates of the control points to support fast searching for neighboring control points. As the average algorithm complexity of the K-D tree search is $O(\log(n))$, the K-D tree-based thinning algorithm leverages the advantages of optimized spatial data structures to efficiently manage and query spatial data. As a consequence, it is able to handle large-scale planetary photogrammetric projects.

2.4. Automatic Identification and Elimination of Invalid Control Points Through Ray Tracing

When a control network is used to perform bundle adjustment, some control points may fail to obtain initial values for the three-dimensional ground coordinates, as shown in Figure 7. This problem is particularly evident in medium- and low-resolution images acquired during the close-range asteroid exploration process, where parts of the image may feature a starry sky in the background. As shown in Figure 7b, although the control points located at the edge of the celestial bodies are nominally valid, their three-dimensional ground coordinates cannot be calculated. Because the geometric accuracy of the initial EO parameters is limited, some control measures may fail to intersect with the existing low-resolution shape of the celestial body. Thus, the initial values for the ground coordinates of these control points are missing. The central premise of bundle adjustment is to calculate the initial values of unknowns. These invalid control points hinder subsequent bundle adjustment and need to be removed before it can be initiated. To this end, the bundle adjustment software tool ‘jigsaw’ within USGS ISIS can provide a prompt message to indicate the presence of such invalid control points in the control network. Then, photogrammetric

engineers can manually remove them based on this prompt. However, only one invalid point can be prompted at a given time during the bundle adjustment process, according to the latest version of USGS ISIS 8.0.0. As before, the existing manual editing method of removing invalid points is very time-consuming.

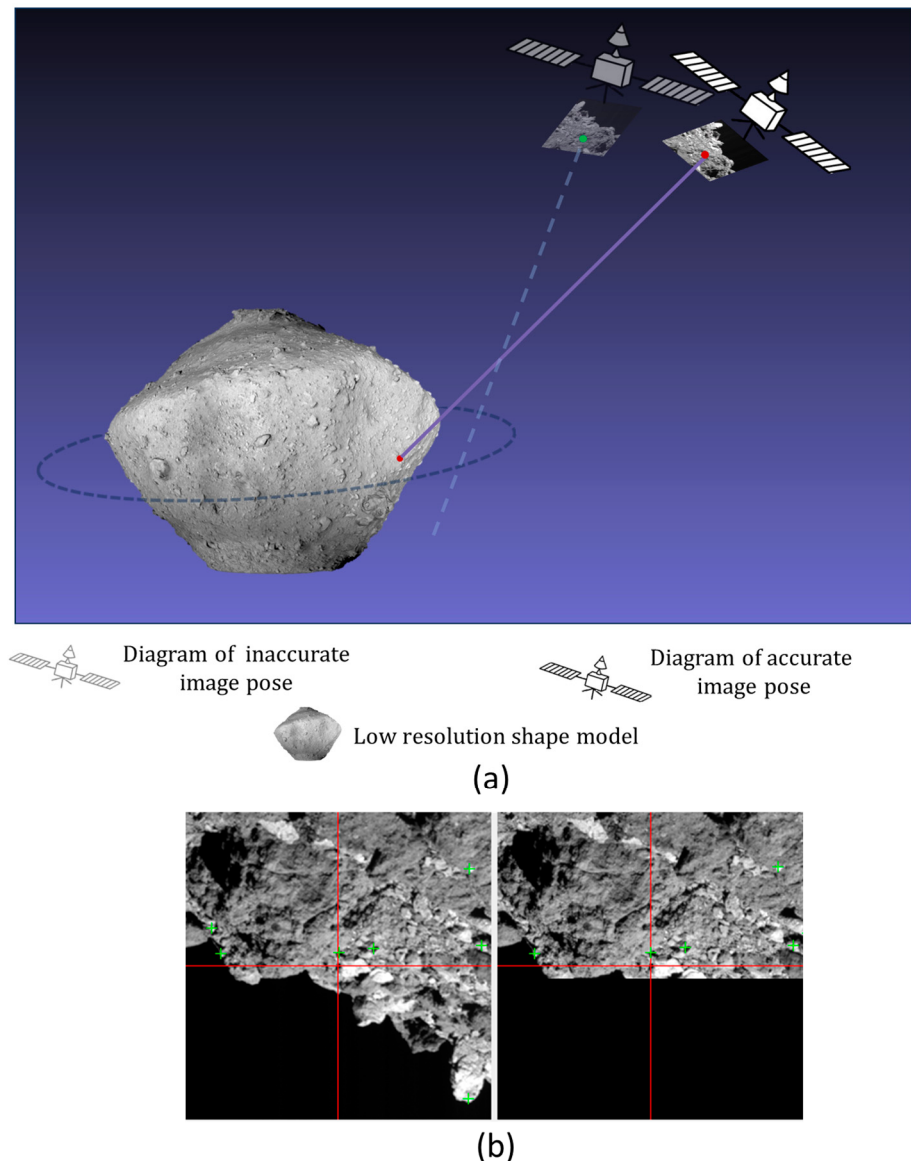


Figure 7. Diagram of invalid control points. (a) When the image's EO parameters are inaccurate, control points near the edge of the valid texture region cannot intersect with the celestial body (The line segments represent the calculated light rays). (b) Illustration of two control measures on asteroid Bennu's surface that cannot intersect the celestial body; the red cross marks indicate the same invalid feature point. The invalid control point fails to compute its ground coordinates due to the low accuracy of the initial EO parameters and the inaccurate shape model of the celestial body (green crosses represent control points).

We propose an algorithm that can automatically identify and remove all invalid control points in a control network, as shown in Figure 8. The algorithm proceeds as follows.

- (1) Input data, such as control network files and existing low-resolution DEM or shape models of the celestial body, are prepared. The camera model is constructed for planetary images.

- (2) Each control point is iterated in order to obtain the corresponding pixel coordinates of each control measure.
- (3) For each control measure, a light ray (look vector) passing through the image point from the camera lens center is computed using the camera model and the pixel coordinates of the control measure.
- (4) Next, this light ray is intersected onto a low-resolution DEM or shape model of the celestial body. The ground coordinates of the intersection's position on the planetary surface are calculated.
- (5) If the light ray does not intersect on the celestial body's ground surface, the control measure or the control point is deemed invalid and should be removed.
- (6) After all control points are processed and invalid control points are removed, a new control network file is generated. It is directly utilized in the subsequent bundle adjustment process.

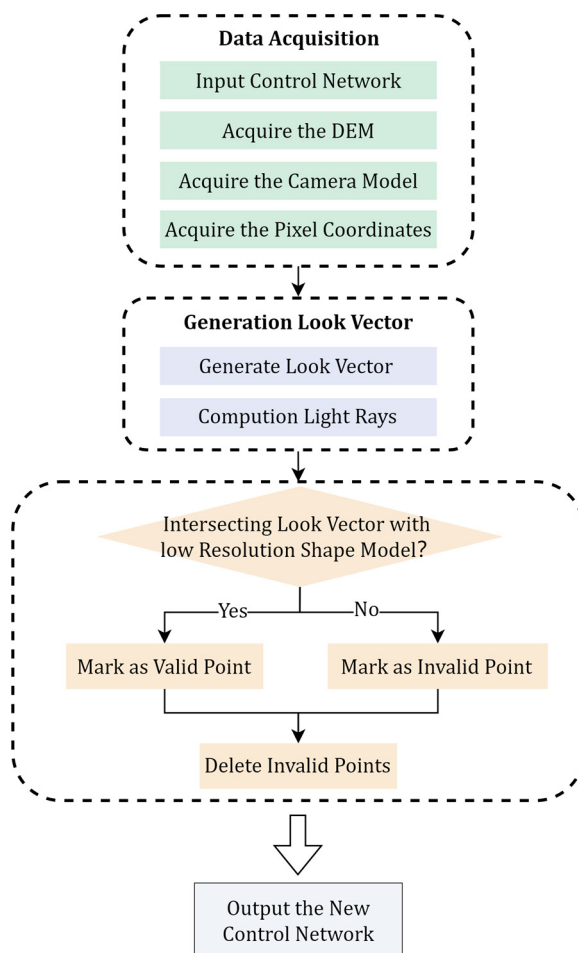


Figure 8. Flowchart for removing invalid control points.

3. Experimental Results

3.1. Data Description

To comprehensively evaluate the effectiveness of the proposed methods, we conducted experiments using three sets of planetary images. The key details of these datasets are shown in Table 1. Dataset 1 consists of 79 LRO NAC images in the LSP. The distribution of images in Dataset 1 is shown in Figure 9. Dataset 2 comprises 32 OSIRIS-REx images of Bennu, with the distribution of these images presented in Figure 10. Dataset 3 includes 9056 OSIRIS-REx Polycam images and covers the entire surface of the asteroid Bennu, as shown in Figure 11. In comparing the results of Dataset 1 and Dataset 3, we may analyze the performance of the proposed method for constructing a control network for different

celestial bodies. Additionally, to examine the effect of implementing the proposed method on small-scale datasets, we conducted a comparative test using Dataset 2 and Dataset 3. The LRO NAC is a line scanner, and the OSIRIS-REx Polycam is a frame camera. Thus, the experiments also consider the applicability of our methods to different types of mapping cameras. The experiments were conducted using a 64-bit Ubuntu 20.04 operating system; the hardware configuration included an Intel Core i7-9700 3.0 GHz CPU and 16 GB of RAM.

Table 1. Main details of images used in our experiments.

| Data Index | Celestial Bodies | Number of Images | GSD (m) | Incidence Angle (Degrees) | Emission Angle (Degrees) | Image Size (Pixels) |
|------------|------------------|------------------|-----------|---------------------------|--------------------------|---------------------|
| Dataset 1 | Moon | 79 | 0.6–1.0 | 85~88 | 1.1~2.2 | 2532 × 52,224 |
| Dataset 2 | Bennu | 32 | 0.047 | 27~40 | 5~35 | 1024 × 1024 |
| Dataset 3 | Bennu | 9056 | 0.02–0.07 | 0~76 | 0~73 | 1024 × 1024 |

Note: GSD refers to ground sample distance.

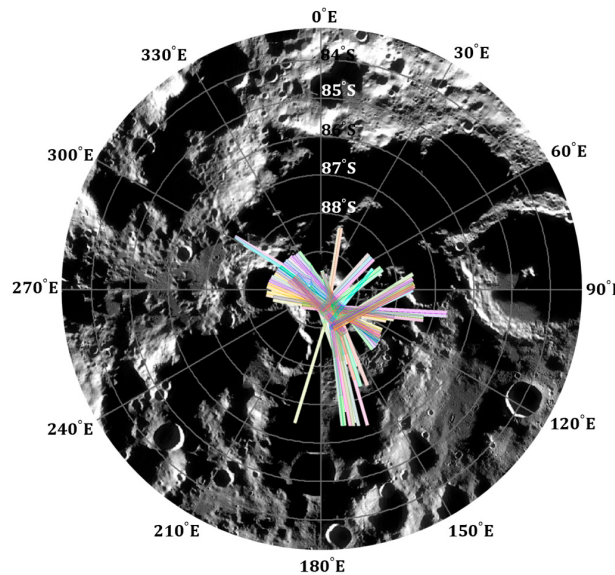


Figure 9. Distribution of images in Dataset 1 over the lunar South Pole (the colored outlines indicate the images, and the base map is the lunar LROC WAC orthoimage provided by NASA [43]).

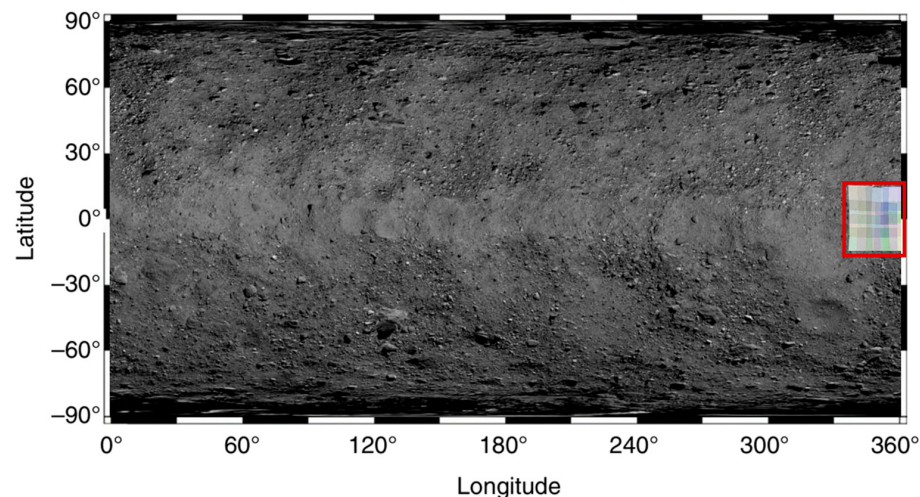


Figure 10. Distribution of images in Dataset 2 (the colored outlines represent the test images, and the base map is the Bennu OSIRIS-REx OCAMS global image mosaic provided by the USGS Astrogeology Science Center [44]).

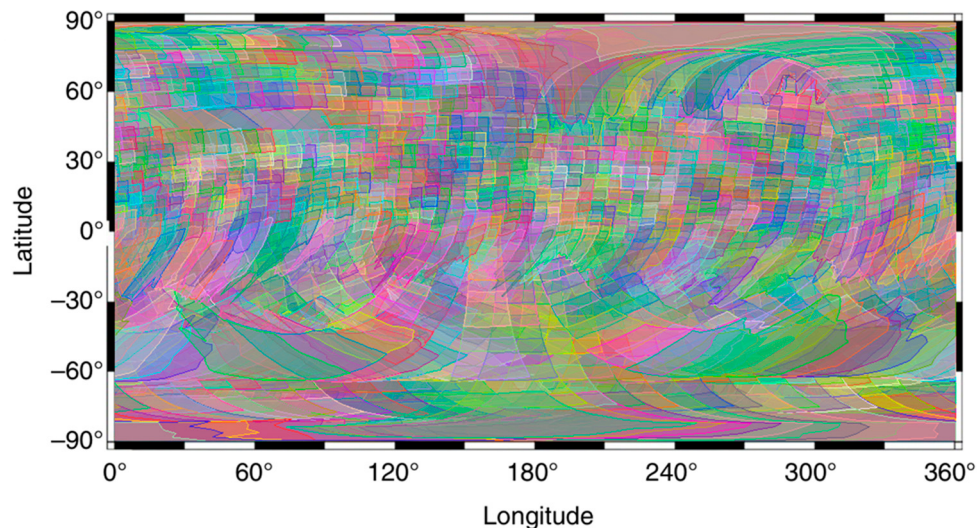


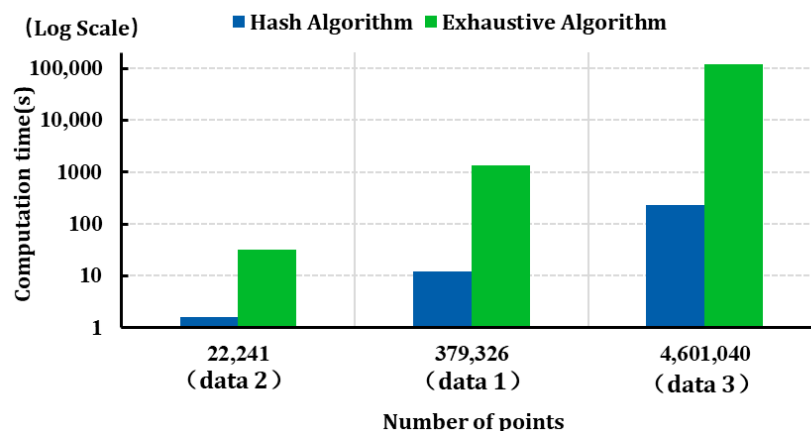
Figure 11. Distribution of images in Dataset 3, covering the entire surface of the asteroid Bennu (the colored outlines represent the images).

3.2. Control Network Construction

We first performed image matching based on approximate orthoimage space for three sets of test data and then converted the pixel coordinates of the matched control points to the original image space. The matched control points were used to generate a control network file by applying both the exhaustive search method and the proposed hash-based method. To support the following bundle adjustment with jigsaw, we adopted the PVL file format used in USGS ISIS to store the generated control network file. The experimental results are presented in Table 2. To provide a more intuitive illustration of how the computation time changes with the data volume, the results are visualized as a statistical graph in Figure 12. Here, we only recorded the processing time needed to build a control network file using the previously matched files and did not include the computation time required for image matching. Notably, there was a significant difference in processing time between the two methods. This difference became more pronounced as the volume of data increased. The computation time of the exhaustive search algorithm was primarily influenced by the number of points in the control network. The control network construction method based on an exhaustive search algorithm demonstrated moderate efficiency when processing a small volume of data, but its efficiency decreased significantly when handling large-scale planetary images. In contrast, the proposed control network construction method based on hash processing exhibited very high efficiency. There are more than 4 million control points in Dataset 3, and the construction of a control network through the proposed hash-based processing method only took 235.67 s. For comparison, the exhaustive search method took 119,472.55 s (about 33 h). Our experimental results therefore demonstrate that the proposed method of constructing a control network can significantly reduce computation time, making it particularly well suited for processing large-scale planetary images. Additionally, it should be noted that there are a very large number of original matching files in Dataset 3 (more than 100,000), and the task of reading such a large number of matching files takes up the majority of the time required for the control network construction through the proposed method.

Table 2. Results of different algorithms in constructing control networks.

| Data Index | Number of Control Points Before Merge | Number of Control Points After Merge | Computation Time(s) | |
|------------|---------------------------------------|--------------------------------------|---------------------|--------|
| | | | Exhaustive | Hash |
| Data 1 | 379,326 | 101,513 | 1341.11 | 12.24 |
| Data 2 | 22,241 | 7747 | 32.23 | 1.59 |
| Data 3 | 4,601,040 | 1,212,391 | 119,472.55 | 235.67 |

**Figure 12.** Time statistics for the construction of a control network using different algorithms. The vertical axis represents the time required to construct the control network. A logarithmic scale is used to enhance the visibility of smaller values due to the significant differences in computation time.

3.3. Control Network Thinning

We performed forward intersection to generate three-dimensional ground coordinates for the control points before initiating the control network-thinning process using the method provided in USGS ISIS alongside our K-D tree-based method. The results of the experiments are shown in Table 3. The results can also be visualized as a statistical graph in Figure 13. The experimental results indicate that the processing time of the USGS ISIS method increases almost exponentially. When tasked with thinning the large-scale control network of Dataset 3, the computation time of the USGS ISIS method exceeded 10 days. The thinning method provided in USGS ISIS is unsuitable for processing such a large-scale control network. In contrast, the proposed method based on the K-D tree only requires a few minutes to thin the control network of Dataset 3. The computational efficiency of the proposed method is much higher than that of USGS ISIS. Figures 14–16, respectively, show the distribution of control points for the three datasets, which result from the thinning process. Figures 14 and 15 also clearly demonstrate that the thinned control network based on our method features a more optimal distribution of control points (with the red box area being more prominent).

Table 3. Results of experiments using different thinning algorithms.

| Data Index | Number of Control Points Before Thinning | Distance Threshold (m) | Computation Time (s) | | Number of Control Points After Thinning | |
|------------|--|------------------------|----------------------|----------|---|----------|
| | | | ISIS | K-D Tree | ISIS | K-D Tree |
| Data 1 | 101,513 | 60 | 6140.29 | 50.36 | 12,458 | 13,872 |
| Data 2 | 7747 | 2 | 34.15 | 4.1 | 1211 | 1523 |
| Data 3 | 1,212,391 | 2 | 881,688.04 | 1277.29 | 164,589 | 191,499 |

Note: As USGS ISIS does not retain key points when thinning dense regions, but the proposed K-D tree algorithm preserves these key points, the results of the two algorithms are not entirely identical.

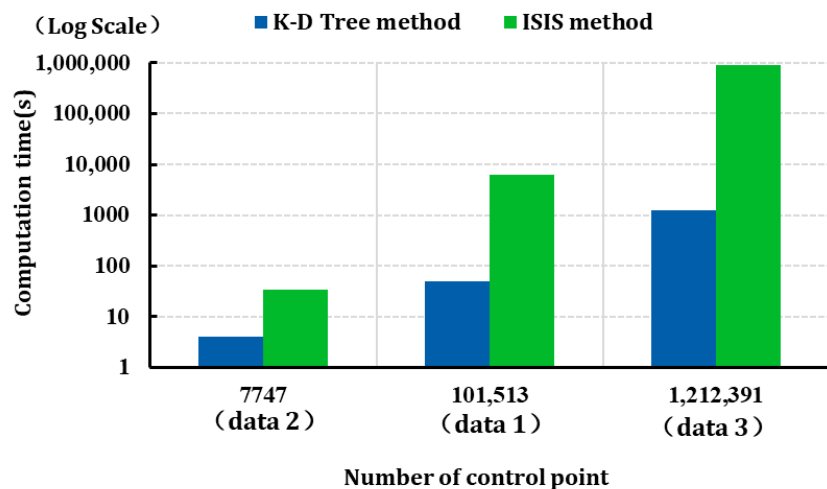


Figure 13. Time statistics for thinning control networks using different algorithms. Similarly, the vertical axis represents computation time (a logarithmic scale is used to enhance the visibility of smaller values due to significant differences in computation time), and the horizontal axis shows the number of control points processed.

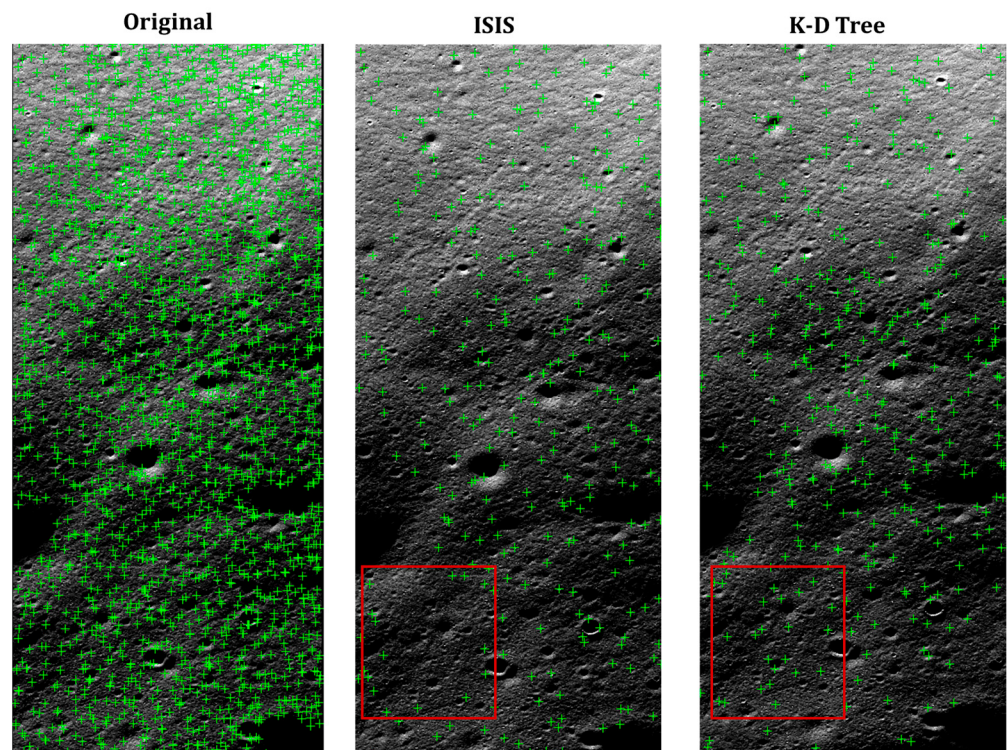


Figure 14. Distribution of control points on the single image before and after thinning the control network of Dataset 1 (green crosses represent control points the red box highlights the differences between the two methods).

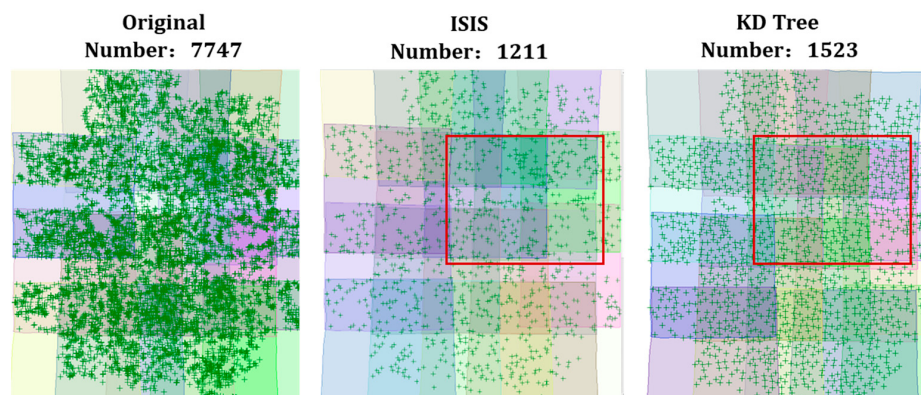


Figure 15. Distribution of control points on each image before and after thinning of the control network of Dataset 2 (areas without control points are due to a lack of overlap between images or poor image quality; green crosses represent control points; the red box highlights the differences between the two methods).

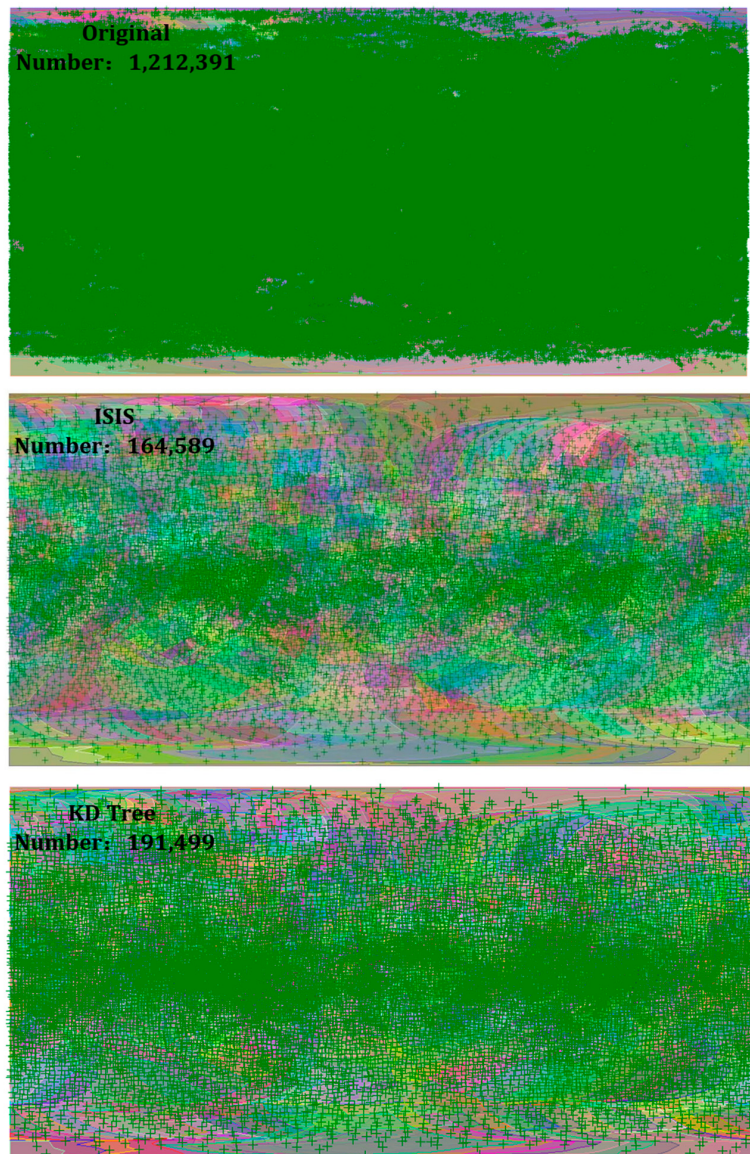


Figure 16. Distribution of control points on each image before and after thinning for the control network of Dataset 3 (the colored outlines represent the images).

3.4. Identification of Invalid Control Points

Some control points on the images of Dataset 3 are located near the edge of the valid texture region (as shown by the red cross marks in Figure 17), and the three-dimensional ground coordinates of these control points cannot be calculated due to failed forward intersection. These invalid control points will therefore prevent subsequent bundle adjustment using jigsaw. Based on the proposed method described in Section 2.4, we automatically identified and removed the invalid control points from the control network of Dataset 3. Ultimately, 3816 invalid control points were found and removed in several minutes. The identified invalid control points within a single image are shown in Figure 17. Another means of eliminating these invalid points is the prompt information provided by jigsaw. However, it can only eliminate one invalid control point at a time, which is extremely cumbersome work.

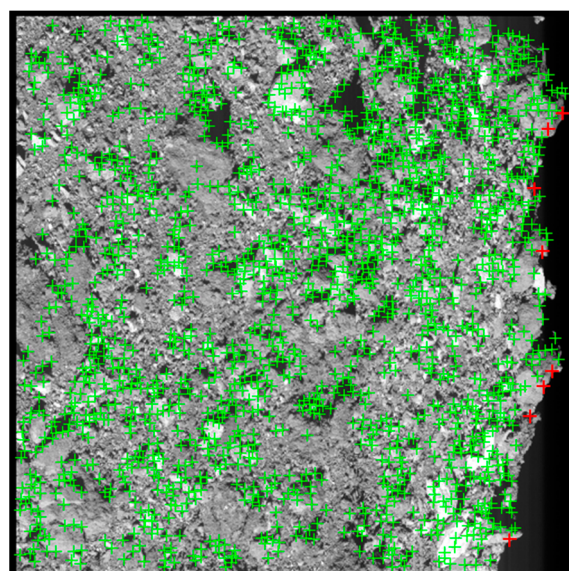


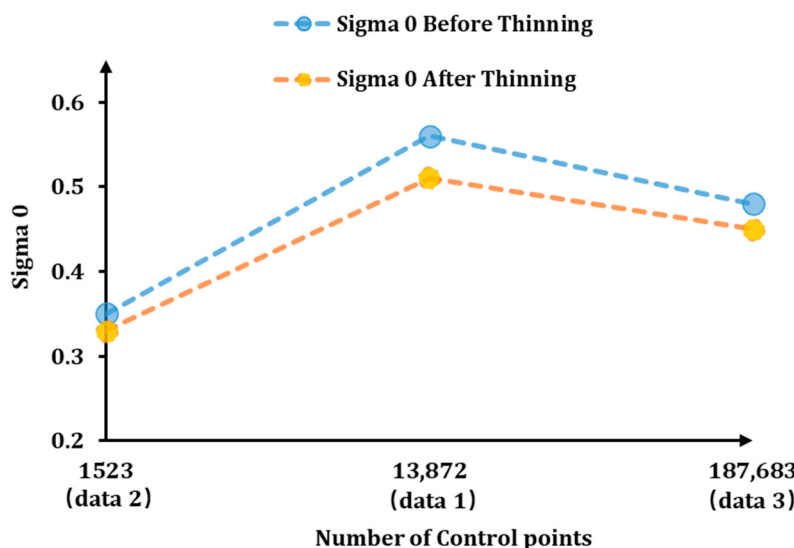
Figure 17. Illustration of the identified invalid control points on a single image from Dataset 3, where the green cross marks represent valid control points, and the red cross marks indicate the invalid control points identified by our method.

3.5. Geometric Accuracy Analysis

We conducted bundle adjustment experiments using the control networks constructed from all the images in the three datasets. This can provide a fair comparison environment for evaluating the bundle adjustment results before and after thinning processing. For Dataset 3, the thinned control points were further processed to eliminate the invalid control points. Then, we performed a comparative analysis of the adjustment results, as shown in Table 4 and Figure 18. The results demonstrate that the thinned control network significantly reduced the iterative processing time required for bundle adjustment as well as preserving geometric accuracy. Generally, sigma 0 is used as an overall index through which to evaluate the results of bundle adjustment. The bundle adjustment results derived from the thinned control network are slightly better than those derived from the original control network. This slight improvement largely results from the removed redundant control points, which may contain large matching errors. To further verify the geometric accuracy of the bundle adjustment results derived from the thinned control network, Figure 19 illustrates the mosaic effects observed in the adjacent orthoimages generated after bundle adjustment. As can be seen, the mosaic error of the adjacent orthophotos is less than 1 pixel. This confirms that our control network-thinning method accomplished high geometric accuracy.

Table 4. BA results before and after thinning.

| Data Index | Number of Control Points | BA Time Before/After Thinning (s) | | Sigma 0 Before/After Thinning | |
|------------|--------------------------|-----------------------------------|---------|-------------------------------|-------|
| | | Before | After | Before | After |
| Data 1 | 13,872 | 282.69 | 86.32 | 0.56 | 0.51 |
| Data 2 | 1523 | 14.37 | 7.47 | 0.35 | 0.33 |
| Data 3 | 187,683 | 7164.67 | 1722.23 | 0.48 | 0.45 |

**Figure 18.** Sigma 0 of the bundle adjustment before and after thinning.**Figure 19.** Image mosaic results of adjacent orthoimages (light blue arrows indicate seam lines).

4. Conclusions

A high-quality control network is fundamental to the photogrammetric processing of planetary remote sensing images. In this paper, we focused on optimizing methods of constructing and editing control networks in planetary photogrammetry. First, we generated approximate orthoimages using the initial EO parameters of the planetary images and obtained control points based on image matching within the orthophoto space. Then, we produced unique hash keys for the control measures based on the designed naming method, and we utilized a hash fast lookup mechanism to accurately and quickly merge control points into the control network. The proposed control network construction method based on hash processing significantly reduced the processing time required to generate a control network from a large number of matching files, thereby outperforming traditional algorithms. Furthermore, to compensate for the redundancy in the initially generated control network, we introduced an efficient control network-thinning algorithm based on a K-D tree structure, which was designed to better support the automatic editing of a large-scale control network and significantly decrease the computation time of the bundle adjustment process. To address the lack of initial values for the ground coordinates

of some invalid points, we proposed an effective algorithm that can automatically identify and remove these invalid points. To validate the feasibility of the proposed methods, we conducted experimental tests using LRO NAC images in the lunar South Pole and OSIRIS-REx PolyCam images covering the vast majority of the asteroid Bennu's surface. Comparison with USGS ISIS demonstrated that our method significantly improved the efficiency and quality of control network construction and reduced the processing time required for bundle adjustment. The final orthophoto mosaics confirm the effectiveness of the proposed algorithms.

The current demand for high-resolution and high-accuracy mapping products of ex-traterrestrial objects is very high, whether they are used to support the implementation of exploration missions or further scientific research. Such demand has prompted improvements in the capacity of planetary photogrammetric processing software. For example, in theory, photogrammetric processing using more than 2 million LRO NAC images can facilitate whole lunar mapping at sub-meter resolution. However, such processing is extremely challenging and therefore beyond the capabilities of existing planetary photogrammetry software such as USGS ISIS 8.0.0 and NASA ASP 3.3.0. The proposed methods of constructing and editing control networks have great potential value in large-scale planetary image processing. In fact, the proposed method of constructing control networks may also serve as a processing framework that can parse matching files generated by other forms of photogrammetric software, thereby enhancing software interoperability in the planetary mapping community. The next step will be to employ Graphics-Processing Unit (GPU) computing and cluster processing technologies to further optimize our algorithms and better support the demands of large-scale planetary image processing.

Author Contributions: Conceptualization, X.G.; methodology, X.G. and X.M.; software, X.G. and X.M.; validation, X.M., X.G. and C.L.; formal analysis, S.W., J.W., P.L., J.Z., Y.W. (Yuying Wang), Z.P., Y.W. (Yinhui Wang) and Q.W.; investigation, T.L.; resources, P.L., J.Z. and X.G.; data curation, X.M. and Q.W.; writing—original draft, X.M.; writing—review and editing, X.G. and C.L.; visualization, Z.P.; supervision, X.G.; project administration, X.G.; funding acquisition, X.G., S.W. and T.L. All authors have read and agreed to the published version of the manuscript.

Funding: This research was funded by the National Natural Science Foundation of China, grant number 42241147; the State Key Laboratory of Geo-Information Engineering, grant number SKLGIE2021-Z-3-1; and the Space Optoelectronic Measurement and Perception Lab, Beijing Institute of Control Engineering, grant number LabSOMP-2023-07; the Open Program of Collaborative innovation Center of Geoinformation Technology for Smart Central Plains Henan Province, grant number 2023C002.

Data Availability Statement: The raw data supporting the conclusions of this article will be made available by the authors upon request.

Acknowledgments: We thank the developers of the open-source planetary remote sensing image processing software (i.e., USGS ISIS 8.0.0 and NASA ASP 3.3.0). We also thank the LRO NAC team for providing planetary images to the public. Special thanks also go to the OSIRIS-REx mission team for their efforts in acquiring and publicizing the Bennu asteroid images.

Conflicts of Interest: The authors declare no conflicts of interest.

References

1. Gwinner, K.; Scholten, F.; Preusker, F.; Elgner, S.; Roatsch, T.; Spiegel, M.; Schmidt, R.; Oberst, J.; Jaumann, R.; Heipke, C. Topography of Mars from Global Mapping by HRSC High-Resolution Digital Terrain Models and Orthoimages: Characteristics and Performance. *Earth Planet. Sci. Lett.* **2010**, *294*, 506–519. [[CrossRef](#)]
2. Wu, B.; Li, F.; Hu, H.; Zhao, Y.; Wang, Y.; Xiao, P.; Li, Y.; Liu, W.C.; Chen, L.; Ge, X.; et al. Topographic and Geomorphological Mapping and Analysis of the Chang'E-4 Landing Site on the Far Side of the Moon. *Photogramm. Eng. Remote Sens.* **2020**, *86*, 247–258. [[CrossRef](#)]
3. Ji, S.; Liu, J.; Lu, M. CNN-Based Dense Image Matching for Aerial Remote Sensing Images. *Photogramm. Eng. Remote Sens.* **2019**, *85*, 415–424. [[CrossRef](#)]
4. Mildenhall, B.; Srinivasan, P.P.; Tancik, M.; Barron, J.T.; Ramamoorthi, R.; Ng, R. NeRF: Representing Scenes as Neural Radiance Fields for View Synthesis. *Commun. ACM* **2022**, *65*, 99–106. [[CrossRef](#)]

5. Pumarola, A.; Corona, E.; Pons-Moll, G.; Moreno-Noguer, F. D-NeRF: Neural Radiance Fields for Dynamic Scenes. In Proceedings of the 2021 IEEE/CVF Conference on Computer Vision and Pattern Recognition (CVPR), Nashville, TN, USA, 20–25 June 2021; pp. 10318–10327. [[CrossRef](#)]
6. Kerbl, B.; Kopanas, G.; Leimkuehler, T.; Drettakis, G. 3D Gaussian Splatting for Real-Time Radiance Field Rendering. *ACM Trans. Graph. (SIGGRAPH)* **2023**, *42*, 139:1–139:14. [[CrossRef](#)]
7. Chen, H.; Hu, X.; Willner, K.; Ye, Z.; Damme, F.; Gläser, P.; Zheng, Y.; Tong, X.; Hußmann, H.; Oberst, J. Neural Implicit Shape Modeling for Small Planetary Bodies from Multi-View Images Using a Mask-Based Classification Sampling Strategy. *ISPRS J. Photogramm. Remote Sens.* **2024**, *212*, 122–145. [[CrossRef](#)]
8. Di, K.; Jia, M.; Xin, X.; Liu, B.; Liu, Z.; Peng, M.; Yue, Z. High Resolution Seamless Dom Generation Over Chang'e-5 Landing Area Using Lroc Nac Images. *Int. Arch. Photogramm. Remote Sens. Spat. Inf. Sci.* **2018**, *XLII-3*, 271–276. [[CrossRef](#)]
9. Acton, C.; Bachman, N.; Semenov, B.; Wright, E. Spice Tools Supporting Planetary Remote Sensing. *ISPRS—Int. Arch. Photogramm. Remote Sens. Spat. Inf. Sci.* **2016**, *XLI-B4*, 357–359. [[CrossRef](#)]
10. Geng, X.; Xu, Q.; Xing, S.; Lan, C. A Generic Pushbroom Sensor Model for Planetary Photogrammetry. *Earth Space Sci.* **2019**, *6*, 1805–1830. [[CrossRef](#)]
11. Smith, D.E.; Zuber, M.T.; Jackson, G.B.; Cavanaugh, J.F.; Neumann, G.A.; Riris, H.; Sun, X.; Zellar, R.S.; Coltharp, C.; Connelly, J.; et al. The Lunar Orbiter Laser Altimeter Investigation on the Lunar Reconnaissance Orbiter Mission. *Space Sci. Rev.* **2010**, *150*, 209–241. [[CrossRef](#)]
12. Edmundson, K.L.; Cook, D.A.; Thomas, O.H.; Archinal, B.A.; Kirk, R.L. Jigsaw: The ISIS3 Bundle Adjustment for Extraterrestrial Photogrammetry. *ISPRS Ann. Photogramm. Remote Sens. Spat. Inf. Sci.* **2012**, *I–4*, 203–208. [[CrossRef](#)]
13. Kim, J.; Lin, S.-Y.; Xiao, H. Remote Sensing and Data Analyses on Planetary Topography. *Remote Sens.* **2023**, *15*, 2954. [[CrossRef](#)]
14. Malin, M.C.; Bell, J.F.; Cantor, B.A.; Caplinger, M.A.; Calvin, W.M.; Clancy, R.T.; Edgett, K.S.; Edwards, L.; Haberle, R.M.; James, P.B.; et al. Context Camera Investigation on Board the Mars Reconnaissance Orbiter. *J. Geophys. Res. Planets* **2007**, *112*, 2006JE002808. [[CrossRef](#)]
15. Robbins, S.J.; Kirchoff, M.R.; Hoover, R.H. Fully Controlled 6 Meters per Pixel Mosaic of Mars's South Polar Region. *Earth Space Sci.* **2020**, *7*, e2019EA001054. [[CrossRef](#)]
16. Liu, P.; Geng, X.; Li, T.; Zhang, J.; Wang, Y.; Peng, Z.; Wang, Y.; Ma, X.; Wang, Q. The Generation of High-Resolution Mapping Products for the Lunar South Pole Using Photogrammetry and Photoclinometry. *Remote Sens.* **2024**, *16*, 2097. [[CrossRef](#)]
17. Chen, C.; Ye, Z.; Xu, Y.; Liu, D.; Huang, R.; Zhou, M.; Xie, H.; Tong, X. Large-Scale Block Bundle Adjustment of LROC NAC Images for Lunar South Pole Mapping Based on Topographic Constraint. *IEEE J. Sel. Top. Appl. Earth Obs. Remote Sens.* **2024**, *17*, 2731–2746. [[CrossRef](#)]
18. Robinson, M.S.; Brylow, S.M.; Tschimmel, M.; Humm, D.; Lawrence, S.J.; Thomas, P.C.; Denevi, B.W.; Bowman-Cisneros, E.; Zerr, J.; Ravine, M.A.; et al. Lunar Reconnaissance Orbiter Camera (LROC) Instrument Overview. *Space Sci. Rev.* **2010**, *150*, 81–124. [[CrossRef](#)]
19. Chin, G.; Brylow, S.; Foote, M.; Garvin, J.; Kasper, J.; Keller, J.; Litvak, M.; Mitrofanov, I.; Paige, D.; Raney, K.; et al. Lunar Reconnaissance Orbiter Overview: The Instrument Suite and Mission. *Space Sci. Rev.* **2007**, *129*, 391–419. [[CrossRef](#)]
20. Veverka, J.; Robinson, M.; Thomas, P.; Murchie, S.; Bell, J.F.; Izemberg, N.; Chapman, C.; Harch, A.; Bell, M.; Carcich, B.; et al. NEAR at Eros: Imaging and Spectral Results. *Science* **2000**, *289*, 2088–2097. [[CrossRef](#)]
21. Lauretta, D.S.; Balram-Knutson, S.S.; Beshore, E.; Boynton, W.V.; Drouet d'Aubigny, C.; DellaGiustina, D.N.; Enos, H.L.; Golish, D.R.; Hergenrother, C.W.; Howell, E.S.; et al. OSIRIS-REx: Sample Return from Asteroid (101955) Bennu. *Space Sci. Rev.* **2017**, *212*, 925–984. [[CrossRef](#)]
22. The OSIRIS-REx Team; Barnouin, O.S.; Daly, M.G.; Palmer, E.E.; Gaskell, R.W.; Weirich, J.R.; Johnson, C.L.; Al Asad, M.M.; Roberts, J.H.; Perry, M.E.; et al. Shape of (101955) Bennu Indicative of a Rubble Pile with Internal Stiffness. *Nat. Geosci.* **2019**, *12*, 247–252. [[CrossRef](#)] [[PubMed](#)]
23. Sokolov, A.I.; Nyrtssov, M.V.; Fleis, M.E.; Nadezhina, I.E. Investigation and Cartographic Representation of Hyperion Space Images Photogrammetric Processing Results. *Planet. Space Sci.* **2024**, *249*, 105945. [[CrossRef](#)]
24. Hartmann, W.; Havlena, M.; Schindler, K. Recent Developments in Large-Scale Tie-Point Matching. *ISPRS J. Photogramm. Remote Sens.* **2016**, *115*, 47–62. [[CrossRef](#)]
25. Li, C.; Zhang, R.; Yu, D.; Dong, G.; Liu, J.; Geng, Y.; Sun, Z.; Yan, W.; Ren, X.; Su, Y.; et al. China's Mars Exploration Mission and Science Investigation. *Space Sci. Rev.* **2021**, *217*, 57. [[CrossRef](#)]
26. Ren, X.; Liu, J.; Li, C.; Li, H.; Yan, W.; Wang, F.; Wang, W.; Zhang, X.; Gao, X.; Chen, W. A Global Adjustment Method for Photogrammetric Processing of Chang'E-2 Stereo Images. *IEEE Trans. Geosci. Remote Sens.* **2019**, *57*, 6832–6843. [[CrossRef](#)]
27. Li, Q.; Huang, H.; Yu, W.; Jiang, S. Optimized Views Photogrammetry: Precision Analysis and a Large-Scale Case Study in Qingdao. *IEEE J. Sel. Top. Appl. Earth Obs. Remote Sens.* **2023**, *16*, 1144–1159. [[CrossRef](#)]
28. Bentley, 2018. ContextCapture. Available online: <https://www.bentley.com/software/contextcapture/> (accessed on 6 October 2024).
29. Agisoft, 2022. Agisoft Metashape: Agisoft Metashape. Available online: <https://www.agisoft.com/> (accessed on 6 October 2024).
30. Schonberger, J.L.; Frahm, J.-M. Structure-from-Motion Revisited. In Proceedings of the 2016 IEEE Conference on Computer Vision and Pattern Recognition (CVPR), Las Vegas, NV, USA, 27–30 June 2016; IEEE: Piscataway, NJ, USA, 2016; pp. 4104–4113. [[CrossRef](#)]

31. Moulon, P.; Monasse, P.; Perrot, R.; Marlet, R. OpenMVG: Open Multiple View Geometry. In *Reproducible Research in Pattern Recognition (RRPR 2016)*; Springer: Cham, Switzerland, 2017; Volume 10214. [[CrossRef](#)]
32. Shen, X.; Li, Q.; Wu, G.; Zhu, J. Bias Compensation for Rational Polynomial Coefficients of High-Resolution Satellite Imagery by Local Polynomial Modeling. *Remote Sens.* **2017**, *9*, 200. [[CrossRef](#)]
33. Grodecki, J.; Dial, G. Block Adjustment of High-Resolution Satellite Images Described by Rational Polynomials. *Photogramm. Eng. Remote Sens.* **2003**, *69*, 59–68. [[CrossRef](#)]
34. Geng, X.; Xu, Q.; Wang, J.; Lan, C.; Qin, F.; Xing, S. Generation of Large-Scale Orthophoto Mosaics Using MEX HRSC Images for the Candidate Landing Regions of China’s First Mars Mission. *IEEE Trans. Geosci. Remote Sens.* **2022**, *60*, 1–20. [[CrossRef](#)]
35. Li, R.; Hwangbo, J.; Chen, Y.; Di, K. Rigorous Photogrammetric Processing of HiRISE Stereo Imagery for Mars Topographic Mapping. *IEEE Trans. Geosci. Remote Sens.* **2011**, *49*, 2558–2572. [[CrossRef](#)]
36. Becker, K.J.; Anderson, J.A.; Weller, L.A.; Becker, T.L. ISIS Support for NASA Mission Instrument Ground Data Processing Systems. In Proceedings of the 44th Lunar and Planetary Science Conference (LPSC), Houston, TX, USA, 18–22 March 2013; Volume 44, p. 2829.
37. Frigeri, A.; Hare, T.; Neteler, M.; Coradini, A.; Federico, C.; Orosei, R. A Working Environment for Digital Planetary Data Processing and Mapping Using ISIS and GRASS GIS. *Planet. Space Sci.* **2011**, *59*, 1265–1272. [[CrossRef](#)]
38. Bland, M.T.; Martin, E.S.; Patthoff, A. Increasing the Usability and Accessibility of Voyager 2 Images of Triton. *Planet. Sci. J.* **2024**, *5*, 112. [[CrossRef](#)]
39. Beyer, R.A.; Alexandrov, O.; McMichael, S. The Ames Stereo Pipeline: NASA’s Open Source Software for Deriving and Processing Terrain Data. *Earth Space Sci.* **2018**, *5*, 537–548. [[CrossRef](#)]
40. Henriksen, M.R.; Manheim, M.R.; Burns, K.N.; Seymour, P.; Speyerer, E.J.; Deran, A.; Boyd, A.K.; Howington-Kraus, E.; Rosiek, M.R.; Archinal, B.A.; et al. Extracting Accurate and Precise Topography from LROC Narrow Angle Camera Stereo Observations. *Icarus* **2017**, *283*, 122–137. [[CrossRef](#)]
41. Lowe, D.G. Distinctive Image Features from Scale-Invariant Keypoints. *Int. J. Comput. Vis.* **2004**, *60*, 91–110. [[CrossRef](#)]
42. Geng, X.; Xu, Q.; Lan, C.; Xing, S.; Hou, Y.; Lyu, L. Orthorectification of Planetary Linear Pushbroom Images Based on an Improved Back-Projection Algorithm. *IEEE Geosci. Remote Sens. Lett.* **2019**, *16*, 854–858. [[CrossRef](#)]
43. Murphy, T.W., Jr.; Adelberger, E.G.; Battat, J.B.R.; Hoyle, C.D.; Johnson, N.H.; McMillan, R.J.; Michelsen, E.L.; Stubbs, C.W.; Swanson, H.E. Laser Ranging to the Lost Lunokhod~1 Reflector. *Icarus* **2011**, *211*, 1103–1108. [[CrossRef](#)]
44. USGS. Astrogeology Science Center. Bennu OSIRIS-REx OCAMS Global PAN Mosaic at 5 cm Resolution. Available online: https://astrogeology.usgs.gov/search/map/bennu_osiris_rex_ocams_global_pan_mosaic_5cm (accessed on 6 October 2024).

Disclaimer/Publisher’s Note: The statements, opinions and data contained in all publications are solely those of the individual author(s) and contributor(s) and not of MDPI and/or the editor(s). MDPI and/or the editor(s) disclaim responsibility for any injury to people or property resulting from any ideas, methods, instructions or products referred to in the content.

Reproduced with permission of copyright owner. Further reproduction
prohibited without permission.